Supporting information

Multifunctional UCNPs@$MnSiO_3$@g-C_3N_4 Nanoplatform: Improved ROS Generation and Reduced Glutathione Levels for High Efficient Photodynamic Therapy

Lili Feng,[†] Fei He,[†,] Yunlu Dai, Shili Gai,[†,]* Chongna Zhong, Chunxia Li,[‡] and Piaoping Yang[†,]*

[†] Key Laboratory of Superlight Materials and Surface Technology, Ministry of Education, College of Material Sciences and Chemical Engineering, Harbin Engineering University, Harbin, 150001, P. R. China [‡] College of Chemistry and Life Sciences, Zhejiang Normal University, Jinhua, 321004, P. R. China

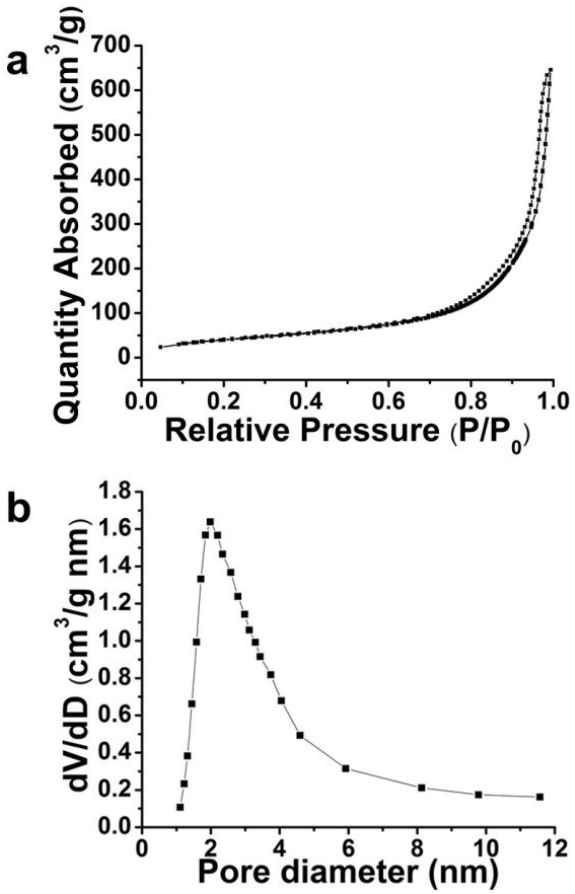

Figure S1. N_2 adsorption/desorption isotherms (a) and pore size distributions (b) of UCNPs@$MnSiO_3$.

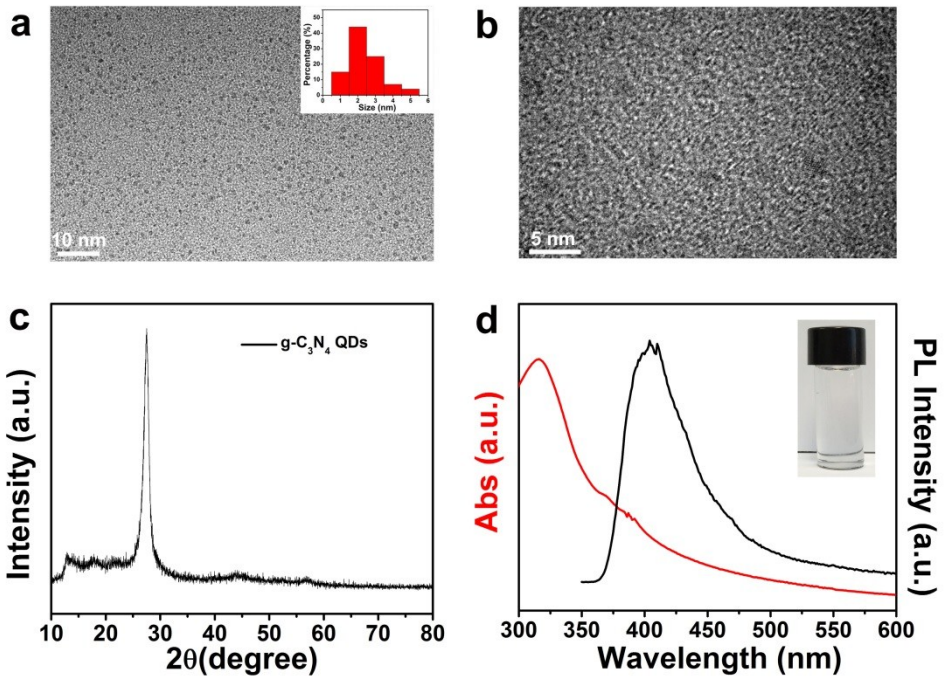

Figure S2. (a) TEM image (scale bar = 10 nm) and particle size distribution (inset) of as-prepared g-C_3N_4 QDs. (b) HRTEM image of g-C_3N_4 QDs. (c) XRD pattern of g-C_3N_4 QDs. (d) The UV-vis absorption spectrum and photoluminescence emission spectrum of g-C_3N_4 QDs irradiation upon UV light (Inset: A digital image of g-C_3N_4 QDs dispersed in pure water).

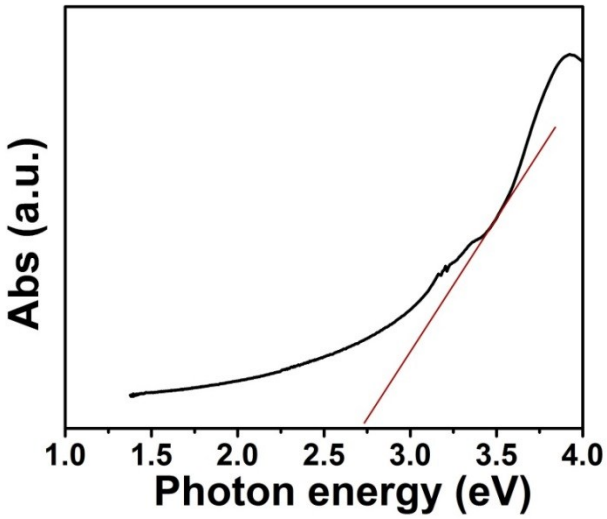

Figure S3. UV-*vis* diffuse reflectance spectra of g-C_3N_4 QDs.

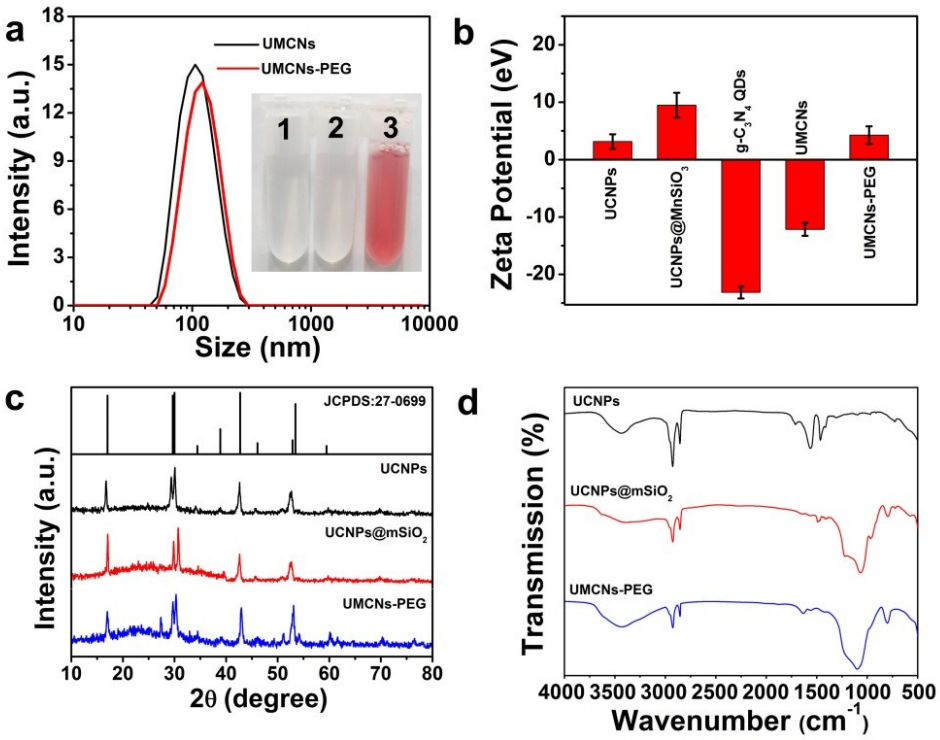

Figure S4. (a) The particle size distributions of UCNPs@$MnSiO_3$@g-C_3N_4, and UMCNs-PEG in water measured by dynamic light scattering (DLS) (inset: the representative photographs of UMCNs-PEG in different solutions including (1) phosphate buffered solution, (2) H_2O and (3) culture medium). (b) Zeta potentials of different sample. (c) XRD patterns and (d) FT-IR spectra of UCNPs (black line), UCNPs@$mSiO_2$ (red line) and UMCNs-PEG (blue line). The standard JCPDS card 27-0699 of $NaGdF_4$.

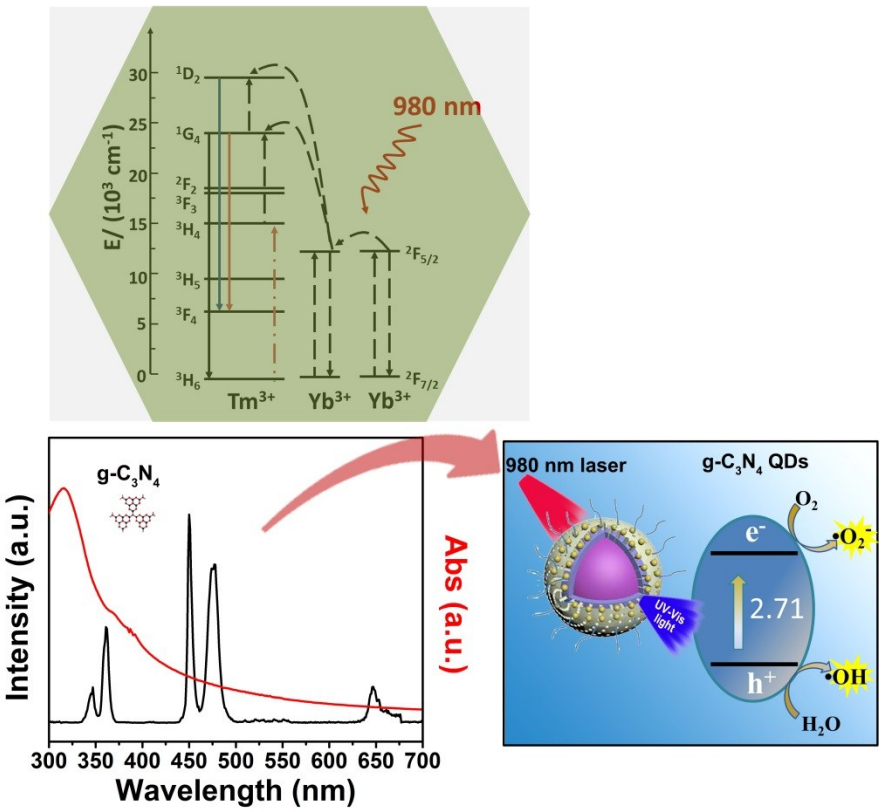

Figure S5. Energy-transfer diagram to explain upconversion emission process of UCNPs. UV-vis absorption apectrum of g-C_3N_4 QDs (Black) and emission spectrum (Red) of UMCNs-PEG upon 980 nm NIR laser excitation and schematic illustration for the ROS generation mechanism of UMCNs-PEG irradiated 980 nm NIR light.

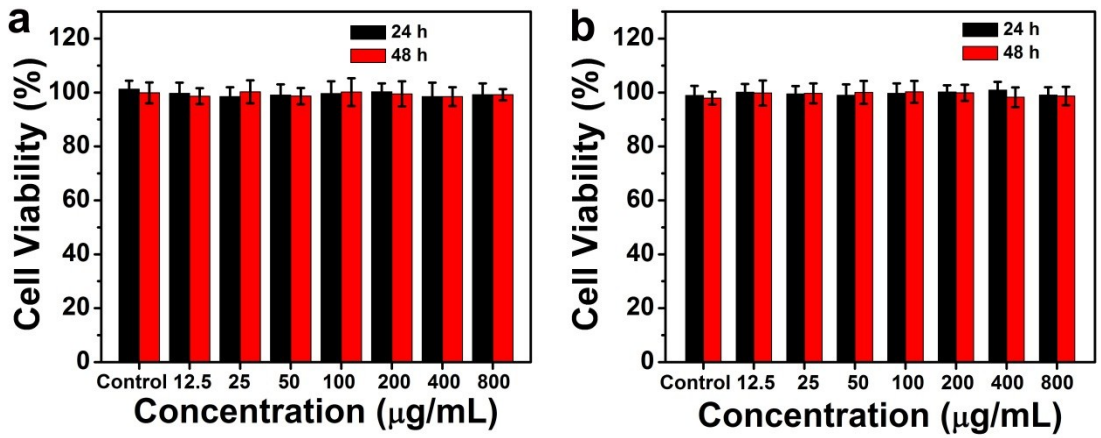

Figure S6. The viability of L929 cells incubated with USCNs-PEG and UMCNs-PEG with different concentrations (800, 400, 200, 100, 50, 25, 12.5 and 0 μg/mL) for 24 h and 48 h measured by MTT assay, respectively.

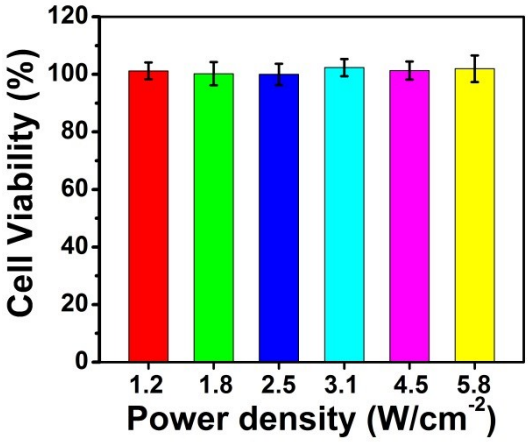

Figure S7. Cell viability after being irradiated with 980 nm laser under different intensities for 30 min (1.2 W cm^{-2}, 5 min break after 5 min irradiation).

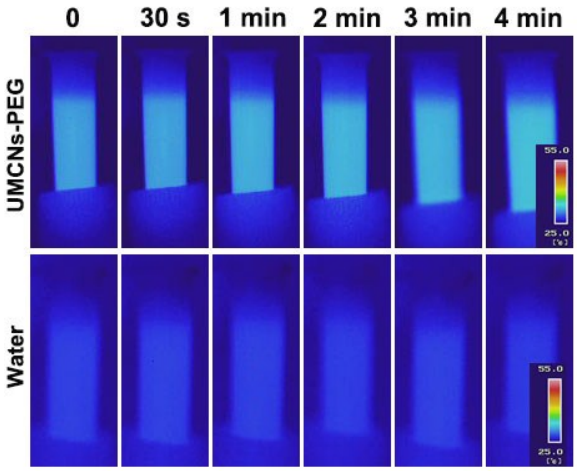

Figure S8. Infrared thermal photographs of UMCNs-PEG (400 μg mL^{-1}) and water exposed to 980 nm NIR laser (1.2 W cm^{-2}) for various times. Note that the samples are dissolved in deionized water.

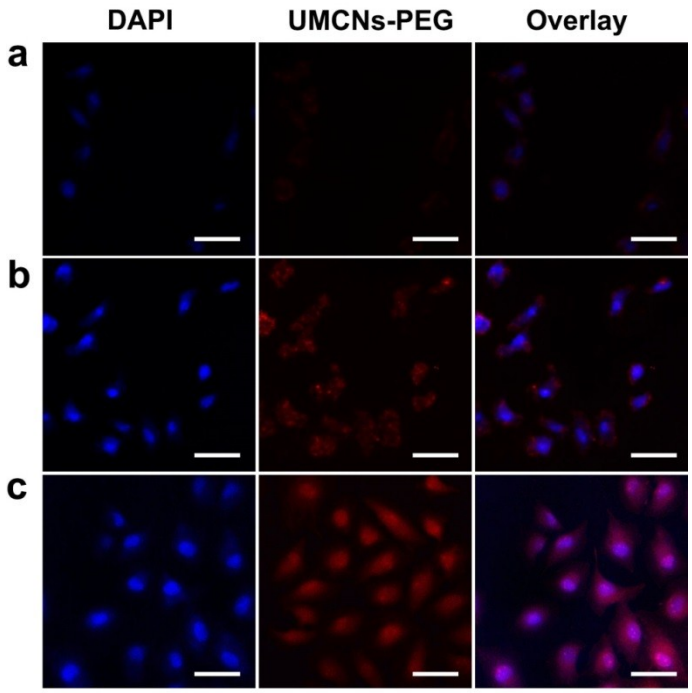

Figure S9. Fluorescence microscopy images of HeLa cells incubated with UMCNs-PEG for 0.5 h (a), 2.5 h (b) and light irradiation after 0.5 h and further 2.5 h of incubation (c). All images were obtained under a magnification of 50 μm.

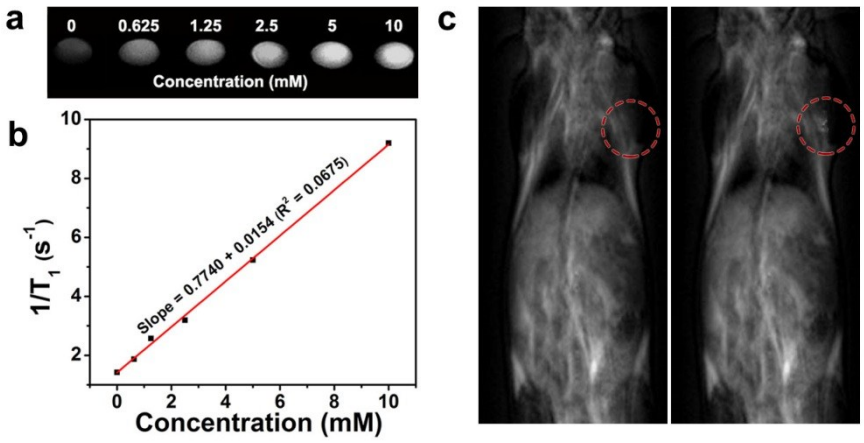

Figure S10. (a) *In vitro* T_1-weighted MR images of UMCNs-PEG at different concentrations. The signal are positively enhanced in a wide concentration range from 0 to 10 mM, (b) Relaxation rate $1/T_1$ as a function of the sample molar concentration. The longitudinal relaxivity (r_1) value of the sample is calculated to be 0.7740 mM^{-1} s^{-1}. T_1-weighted MRI images of a tumor-bearing Balb/c mouse, (c) pre injection and (d) after injection *in situ*. The tumor site exhibits much higher MRI singal intensity after injection, illustrating that UMCNs-PEG could be used as a promising contrast agent for T_1-weighted MR imaging.

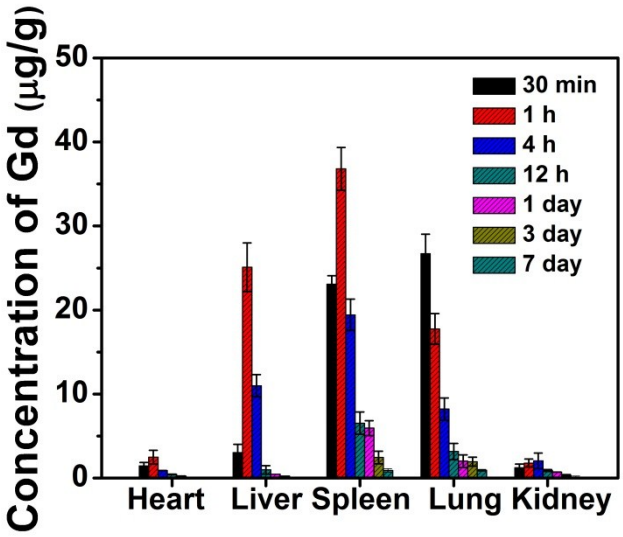

Figure S11. The bio-distribution of Gd in major organs of mice after injection of UMCNs-PEG intravenously at different time points. Error bars indicate standard deviations, N = 4.

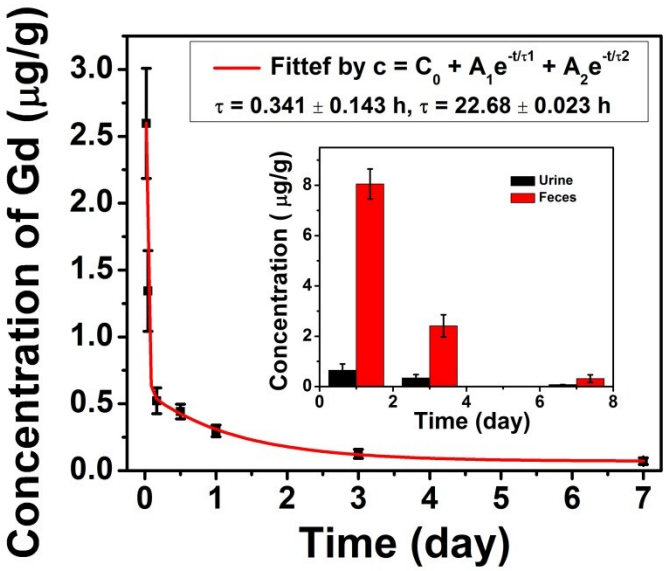

Figure S12. The blood circulation time in tumor-bearing mice after intravenous injection of UMCNs -PEG, inset is the metabolism concentration with different times.